Dynamic spin susceptibility of paramagnetic spinel LiV_2O_4

V. Yushankhai,[1,2] A. Yaresko,[1] P. Fulde,[1] and P. Thalmeier[3]

[1]*Max-Planck-Institut für Physik Komplexer Systeme, D-01187 Dresden, Germany*
[2]*Joint Institute for Nuclear Research, 141980 Dubna, Russia*
[3]*Max-Planck-Institut für Chemische Physik fester Stoffe, D-01187 Dresden, Germany*

In an attempt to explain inelastic neutron scattering data for LiV_2O_4, the dynamical spin susceptibility $\chi(\mathbf{Q}, \omega)$ at zero temperature is calculated. The starting point is a weak coupling approach based on the local-density approximation band structure for that material. It is supplemented by a random-phase approximation treatment of local on-site interactions and contains an adjustable parameter. Due to the geometrically frustrated lattice structure, the magnetic response is strongly enhanced in the vicinity of a nearly spherical surface in $\mathbf{Q}$ space. We compare these results with recent low-temperature neutron scattering data. The measured spin relaxation rate Γ is used to estimate the spin-fluctuation contribution to the specific heat.

PACS number(s): 71.27.+a, 71.10.Fd, 71.30.+h

I. INTRODUCTION

The metallic spinel LiV_2O_4 has been identified as the first $3d$ system with heavy quasiparticles.[1–3] The low-temperature specific heat coefficient $\gamma = C/T \simeq 0.4$ J mol^{-1} K^{-2} is considerably enhanced as compared with that of simple metals, and the same holds true for the spin susceptibility χ_S. For high temperatures, $T > 50$ K, the latter shows a Curie-Weiss behavior, $\chi_S(T) = \chi_0 + C/(T + \theta)$, where the Curie constant $C = 0.47$ cm^3 $K/($mol V$)$ and the Weiss temperature $\theta = 63$ $K > 0$ implies an antiferromagnetic interaction between the V ions. No magnetic ordering has been observed down to 0.02 K.[1] Concerning the entropy $S(T)$ whose temperature dependence is determined from the specific heat, one finds that $S(T = 60$ $K) - S(0) \simeq 10$ J$/($mol $K)$, which is close to $2R \ln 2$, where R denotes the gas constant. Thus, at 60 K, there is nearly one excitation per V ion. This strongly suggests that the low-lying excitations, which lead to the heavy quasiparticle behavior, result from spin degrees of freedom. Needless to say that the original discovery of the heavy quasiparticles in LiV_2O_4 has initiated many subsequent experimental studies including transport, nuclear magnetic resonance (NMR),[4,5] muon spin relaxation (μSR),[6] photoelectron spectroscopy (PES),[7] and inelastic neutron scattering work.[8–10] A special feature of the spinels and hence of LiV_2O_4 is that the V ions occupy the sites of a pyrochlore lattice. The latter consists of corner sharing tetrahedra. For a microscopic understanding of the observed heavy quasiparticle behavior with an average number $n_d = 1.5$ of d electrons per V ion, two different approaches starting from either a strong or a weak coupling limit are possible. They have been reviewed in Ref. 11, and we want to discuss them briefly now.

Density functional calculations based on the local-density approximation (LDA) demonstrate that electrons near the Fermi energy E_F are of t_{2g} character.[12–14] The calculated density of states within LDA is too small by a factor of 25 in order to explain the large γ coefficient. Therefore, in Ref. 15, the limit of strong correlations was taken as a starting point. In that limit, charge fluctuations between V ions are strongly suppressed due to both the on-site and nearest neighbor intersite electron Coulomb repulsions.[16] Thus, in the ground state, slowly varying charge configurations include V sites that are either singly (spin $1/2$) or doubly (spin 1) occupied. In the latter case, $S = 1$ is due to the Hund's rule. The ground state consists of configurations in which the spin-$1/2$ and spin-1 sites form two subsets of chains (rings), and the spin chains are effectively decoupled because of geometrical frustration in the pyrochlore lattice. Within this spin chain model, the nearest neighbor (nn) exchange couplings J_{nn} are assumed only. The linear specific heat coefficient $\gamma = 2k_BR/3J_{nn}$, where k_B is the Boltzmann constant, of the spin-$1/2$ chains is found to be large. Only a factor of 2 is missing as compared with experiment. Here, $J_{nn} \simeq 3$ meV is the nn spin-$1/2$ chain coupling, as obtained from LDA$+U$ calculations. The spin-1 chains with a gapped spectrum do not contribute to γ coefficient. Our recent analysis has shown, however, that in the model formulation, the next-nearest neighbor (nnn) coupling J_{nnn} cannot be excluded, which may lead to a considerable renormalization of the above estimate of γ. Moreover, if $J_{nnn}/J_{nn} > 0.24$, the spin-$1/2$ chain system may even enter the regime of dimerization. Of course, effects of the kinetic energy which were omitted so far should also be included in an extended spin chain model.

Because of these growing complications, it is of interest to investigate what results for the spin correlations are, when one starts from the limit of weak correlations instead. In this limit, the d electrons are in broad LDA energy bands in contrast to nearly localized electronic states in the opposite limit. Since the effects of electron Coulomb repulsions are neglected (except for those already contained in the LDA), the geometrically frustrated lattice structure plays a role only as it affects the form of the LDA energy bands. As shown below, this results, however, in a characteristic form of the $\mathbf{Q}$ dependence of the unenhanced dynamic spin susceptibility $\chi^{(0)}(\mathbf{Q}, \omega)$. So, the starting points of both approaches are very different. The hope is that both limits can eventually brought to convergence in a region which is between the two limiting situations.

The present work was first motivated by results of quasielastic neutron scattering measurements[8–10] carried out on polycrystalline samples of LiV_2O_4. At low temperatures,
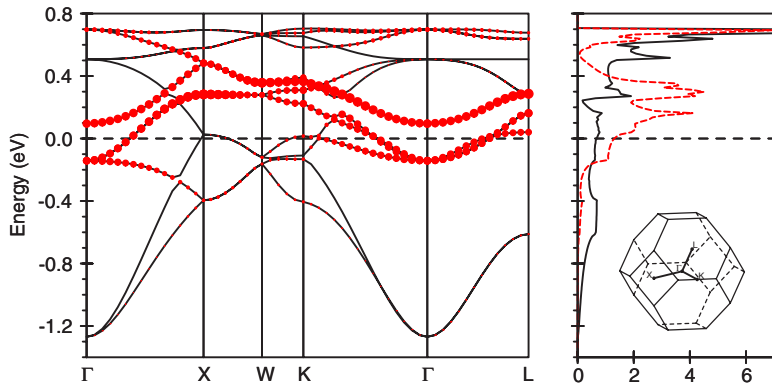
FIG. 1. (Color online) LDA bands originating from V da_{1g} and e'_g states (left panel) and orbital resolved densities of states per eV, per V atom (right panel). Densities of a_{1g} and e'_g states are plotted by dashed and solid lines, respectively. The size of circles in the left panel is proportional to the weight of the a_{1g} orbital in the state. The Fermi energy is at zero.

strong quasielastic neutron scattering was found in a range of wave vectors, $0.4 \text{ Å}^{-1} \lesssim Q \lesssim 0.8 \text{ Å}^{-1}$. The quasielastic linewidth $\Gamma(Q)$ is of a few meV, indicating a slow spin dynamics in the above Q region. Because of the relation between the measured dynamic structure factor and the imaginary part of the dynamic spin susceptibility $S(\mathbf{Q}, \omega; T) = (1 - e^{-\hbar\omega/k_B T})\chi''(\mathbf{Q}, \omega; T)$, calculation of $\chi(\mathbf{Q}, \omega; T)$ is of fundamental importance to interpret inelastic neutron scattering data.

Our aim is to include a realistic electronic band structure for LiV_2O_4 into random-phase approximation (RPA) like calculations of the dynamic spin susceptibility. The latter is enhanced due to exchange-correlation effects of electrons on the vanadium $3d$ orbitals. The calculations are performed for $T = 0$. We restrict ourselves to the study of $\chi(\mathbf{Q}, \omega)$ along high-symmetry directions in the reciprocal space and focus on the analysis of its low-frequency behavior. As shown below, even such a restricted consideration allows us to gain insight into the low-temperature spin dynamics of LiV_2O_4 and provides a basis for a comparison of computational results with experimental data. Our main findings are the following: (i) the dominant maxima of the calculated unenhanced spin susceptibility $\chi^{(0)}(\mathbf{Q}, \omega)$, i.e., the one from LDA occur in the same region of $\mathbf{Q}$ space where the largest intensity of the inelastic neutron scattering is found, and (ii) a moderate value of the electronic local exchange-correlation coupling $\mathcal{K}$ is sufficient within RPA to bring the system close to a magnetic instability and thus to a strong slowing down of spin fluctuations for wave vectors $\mathbf{Q}$ determined by (i).

Because we assume local, Hubbard-like electron interactions, the exchange-correlation coupling $\mathcal{K}$ is $\mathbf{Q}$ independent and therefore treated here as an orbital-independent adjustable parameter. Along the way, we will discuss possible extensions of the theory in some detail but not pursue them further.

The random-phase approximation was applied to the one-band Hubbard model by Izuyama *et al.* in their seminal work[17] and developed further by Doniach.[18] The multiband generalization of the RPA to the dynamic spin susceptibility adopted here is in a close relation with earlier works by Cook[19] and Callaway *et al.*[20,21] We also mention papers by Stenzel and Winter[22,23] along that line. The connection with these works will be pointed out at various places in the discussion below.

We also address the problem of spin-fluctuation contribution γ_{sf} to the low-temperature specific heat coefficient γ. As

known,[24–26] slow spin-fluctuation dynamics can be described approximately by a system of overdamped oscillators. In general, these oscillators are characterized by $\mathbf{Q}$-dependent spin relaxation rates $\Gamma_\mathbf{Q}$. Based on the available inelastic neutron scattering data[8–10] and our RPA calculation of $\chi(\mathbf{Q}, \omega)$ in LiV_2O_4, we suggest below a model describing a particular distribution of $\Gamma_\mathbf{Q}$ in $\mathbf{Q}$ space. Then, we show that a diversity of experimentally determined values of $\Gamma_\mathbf{Q}$ leads to a theoretical estimate for γ_{sf} that falls also into a broad range with the largest value being close to γ observed in experiment.

A similar RPA approach to a fluctuation mechanism in LiV_2O_4 based on a tight binding model for the V $3d$ bands has been proposed in Ref. 27 in an attempt to explain the specific heat enhancement. The numerical calculations have been performed for the supersymmetric case where all spin and/or orbital fluctuations are controlled by the same nearly critical interaction parameter. In the numerical calculations, the instability is obtained only around the center of the Brillouin zone, and the large mass enhancement is due to contributions from all possible spin and/or orbital fluctuations at $\mathbf{Q} = 0$. In our approach, we take the complementary viewpoints that (i) only the spin fluctuations are close to be critical and (ii) the critical spin fluctuations at $T = 0$ are located in a wide region of $\mathbf{Q}$ space far away from the Brillouin zone center in accord with the experimental evidence from inelastic neutron scattering. Thus, in our model, the extended region of nearly critical spin fluctuations in momentum space is a promising candidate for the large mass enhancement.

II. ELECTRONIC BAND STRUCTURE AND UNENHANCED DYNAMIC SPIN SUSCEPTIBILITY OF LiV₂O₄

To define a reciprocal lattice for the cubic spinel structure of LiV_2O_4, it is convenient first to introduce the orthogonal basis vectors $\mathbf{G}^{(\alpha)}$, $(\alpha = x, y, z)$, of the length $a^* = 2\pi/a \simeq 0.76 \text{ Å}^{-1}$; here, $a = 8.23 \text{ Å}$ is the lattice parameter.[3] The irreducible Brillouin zone (BZ) of the underlying fcc lattice is a polyhedron depicted in Fig. 1, where X, Y, and Z points on their faces are given by the end points of the vectors $\pm\mathbf{G}^{(\alpha)}$. A cube that encloses the polyhedron provides us with a larger cubic BZ most appropriate in characterizing the periodic properties of $\chi(\mathbf{Q}, \omega)$ in $\mathbf{Q}$ space. An arbitrary wave vector $\mathbf{Q}$ will be denoted by $\mathbf{Q} = \mathbf{q} + \mathbf{G}$, where $\mathbf{q}$ belongs to

the first cubic BZ and $\mathbf{G}$ is a reciprocal-lattice vector; $\mathbf{G} = 2\Sigma_\alpha n_\alpha \mathbf{G}^{(\alpha)}$, where n_α are integers.

In the present work, the band structure for LiV_2O_4 is calculated within the LDA in the framework of linear muffin tin orbitals and using the atomic sphere approximation. The main features of the calculated band structure agree well in many details with the LDA results obtained by other authors.[12–14]

In LiV_2O_4, the vanadium 3d bands and the oxygen 2p bands are well separated by an energy of ~ 2 eV. The octahedral component of the crystal field is strong enough to split the vanadium 3d bands into two separate and nonoverlapping bands originating from t_{2g} and e_g orbitals. A weak trigonal component of the crystal field produces a further splitting of the low-lying set of t_{2g} orbitals into $(a_{1g}+e_g')$ orbitals. The latter dominate the electronic states near the vicinity of the Fermi energy. The complexity of the band structure results in many sheets of the Fermi surface.

Recalling that LiV_2O_4 is found to be a paramagnet down to very low temperatures, we assume that the system remains spin disordered at all temperatures and carry out a calculation of the dynamic spin susceptibility for $T=0$. Without external magnetic field, the longitudinal and the transverse susceptibility are the same.

In the multiband model under consideration, the time- and space-Fourier transforms of the dynamic spin susceptibility for the LDA band electrons take the following familiar forms

$$\chi^{(0)}_{\mathbf{G},\mathbf{G}'}(\mathbf{q},\omega) = \frac{1}{V}\sum_{\eta,\eta'}\sum_{\mathbf{k}}\gamma_{\eta'\eta}(\mathbf{k},\mathbf{q};\omega)\langle\mathbf{k}-\mathbf{q}/2,\eta|e^{-i(\mathbf{q}+\mathbf{G})\mathbf{r}}|\mathbf{k}$$
$$+\mathbf{q}/2,\eta'\rangle\langle\mathbf{k}+\mathbf{q}/2,\eta'|e^{i(\mathbf{q}+\mathbf{G}')\mathbf{r}}|\mathbf{k}-\mathbf{q}/2,\eta\rangle,$$
$$(1)$$

$$\gamma_{\eta'\eta}(\mathbf{k},\mathbf{q};\omega) = -\frac{f_{\eta'}(\mathbf{k}+\mathbf{q}/2)-f_\eta(\mathbf{k}-\mathbf{q}/2)}{E_{\eta'}(\mathbf{k}+\mathbf{q}/2)-E_\eta(\mathbf{k}-\mathbf{q}/2)+\hbar\omega+i\delta}.$$
$$(2)$$

In Eqs. (1) and (2), the plane-wave matrix elements are calculated on the basis of Bloch functions $\psi_{\mathbf{k}\eta}(\mathbf{r})$, with the band index η and energy $E_\eta(\mathbf{k})$. Here, $f_\eta(\mathbf{k})$ is the Fermi distribution function.

In the next section, the exchange-correlation enhanced spin susceptibility $\chi_{\mathbf{G},\mathbf{G}'}(\mathbf{q},\omega)$ is derived within the RPA. In this derivation, $\mathbf{G}\neq\mathbf{G}'$ matrix elements of $\chi^{(0)}_{\mathbf{G},\mathbf{G}'}(\mathbf{q},\omega)$ are involved, which lead to the well known problem of large matrix inversion. Since the magnetically active 3d orbitals of vanadium ions are rather compact, a large set of the reciprocal-lattice vectors $\mathbf{G}$ has to be taken into account and thus a matrix $\chi^{(0)}_{\mathbf{G},\mathbf{G}'}(\mathbf{q},\omega)$ of high dimension has to be inverted. One encounters a similar problem when calculating the inverse dielectric matrix for electrons in transition metals.[28] To overcome this difficulty, an elegant procedure based on a simple and reliable approximation has been proposed and developed by several authors.[21,28] We are now in a position to discuss some preliminaries of this procedure, the

central point of which is the search for a separable form for the plane-wave matrix elements entering Eq. (1).

Taking into account a four-site basis within the primitive lattice cell, there are altogether 12 bands of dominant d character, which originate from partially occupied $a_{1g}+e_g'$ orbitals of the vanadium ions. Therefore, one expects that the Bloch functions $\psi_{\mathbf{k}\eta}(\mathbf{r})$ for the actual d bands near the Fermi energy can be well described by the orbital basis set $\phi_{\mathbf{k},\tau m}$ of Bloch functions defined in terms of atomiclike $a_{1g}+e_g'$ orbitals localized on the pyrochlore lattice sites $\mathbf{j}+\tau$:

$$\phi_{\mathbf{k},\tau m} = \frac{1}{\sqrt{N}}\sum_{\mathbf{j}}e^{i\mathbf{k}\mathbf{j}}w_m(\mathbf{r}-\mathbf{j}-\tau).$$
$$(3)$$

Here, the sum is over N $\mathbf{j}$ sites of the underlying fcc lattice. The τ vectors form a four-point basis. Furthermore, $w_m(\mathbf{r}-\mathbf{j}-\tau)$ is the mth orbital from the $a_{1g}+e_g'$ orbital set on the pyrochlore lattice site $\mathbf{j}+\tau$. For shortening the notation, we use below a composite index (τm) to refer to $w_m(\mathbf{r}-\mathbf{j}-\tau)$ as the (τm)th orbital belonging to the $\mathbf{j}$th primitive lattice cell. We recall the following unitary transformation between the band and the orbital representations for Bloch functions:

$$\psi_{\mathbf{k}\eta}(\mathbf{r}) = \sum_{\tau m}a_{(\tau m)\eta}(\mathbf{k})\phi_{\mathbf{k},\tau m}.$$
$$(4)$$

Here, $a_{(\tau m)\eta}(\mathbf{k})$ are elements of the (12×12) matrix satisfying the following orthogonality and completeness relations:

$$\sum_{\tau m}a^*_{(\tau m)\eta}(\mathbf{k})a_{(\tau m)\eta'}(\mathbf{k}) = \delta_{\eta\eta'},$$

$$\sum_\eta a_{(\tau m)\eta}(\mathbf{k})a^*_{(\tau'm')\eta}(\mathbf{k}) = \delta_{\tau m,\tau'm'},$$
$$(5)$$

where δ is the Kronecker symbol. The plane-wave matrix elements in Eq. (1) can now be written as

$$\langle\mathbf{k}+\mathbf{q}/2,\eta'|e^{i(\mathbf{q}+\mathbf{G}')\mathbf{r}}|\mathbf{k}-\mathbf{q}/2,\eta\rangle$$
$$= \sum_{\tau'm'}\sum_{\tau m}A^{\eta'\eta}_{(\tau'm')(\tau m)}(\mathbf{k},\mathbf{q})\mathcal{F}_{(\tau'm')(\tau m)}(\mathbf{k},\mathbf{q}+\mathbf{G}'),$$
$$(6)$$

where

$$A^{\eta'\eta}_{(\tau'm')(\tau m)}(\mathbf{k},\mathbf{q}) = a^*_{(\tau'm')\eta'}(\mathbf{k}+\mathbf{q}/2)a_{(\tau m)\eta}(\mathbf{k}-\mathbf{q}/2),$$
$$(7)$$

while the form factor $\mathcal{F}$ involves integrals over pairs of w_m orbitals localized either at the same site or at two different lattice sites. The compactness of these orbitals suggests neglecting the two-center integrals, which leads to the following approximation for the form factor:

$$\mathcal{F}_{(\tau'm')(\tau m)}(\mathbf{k},\mathbf{q}+\mathbf{G}) \simeq \delta_{\tau'\tau}e^{i(\mathbf{q}+\mathbf{G})\tau}\int d\mathbf{r}w_{m'}(\mathbf{r})e^{i(\mathbf{q}+\mathbf{G})\mathbf{r}}w_m(\mathbf{r})$$

$$= \delta_{\tau'\tau}F_{(\tau m')(\tau m)}(\mathbf{q}+\mathbf{G}).$$
$$(8)$$

We have checked that the neglect of the overlap integrals between the calculated d orbitals on different sites in LiV_2O_4 is a rather accurate approximation. The approximation results, in particular, in a $\mathbf{k}$ independence of the form factor F in Eq. (8), the advantage of which will be exploited in the
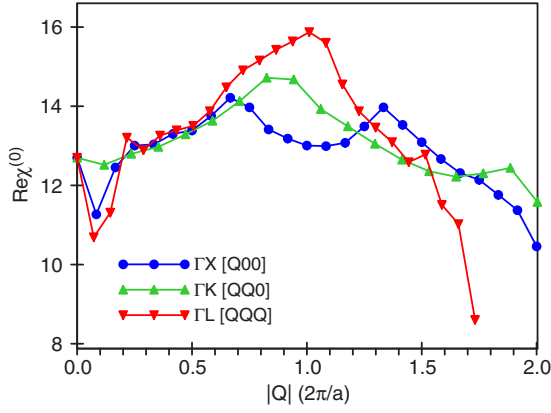
FIG. 2. (Color online) Unenhanced static spin susceptibility $\chi^{(0)}(\mathbf{Q},0)$, in states per eV, per primitive cell (four V atoms), calculated along high-symmetry directions as a function of $|\mathbf{Q}|$.

next section. It is worth noting that in Eq. (8), the factors $e^{i(\mathbf{q}+\mathbf{G})\tau}$ are invariant under translations by $2\mathbf{G}$ in reciprocal space.

For shortening the notation, it is helpful to replace in the upper equations the double "orbital" index $(\tau'm')(\tau m)$ by a symbol L and to introduce the following orbitally projected expression:

$$\gamma_{LL'}(\mathbf{q},\omega) = \frac{1}{N} \sum_{\eta,\eta'} \sum_{\mathbf{k}} [A_L^{\eta'\eta}(\mathbf{k},\mathbf{q})]^* \gamma_{\eta'\eta}(\mathbf{k},\mathbf{q};\omega) A_{L'}^{\eta'\eta}(\mathbf{k},\mathbf{q}).$$
(9)

In the following, the left-hand side of Eq. (9) is referred to as the matrix γ in the orbital L representation. The elements of the orbital γ matrix are periodic in reciprocal space: $\gamma_{LL'}(\mathbf{q}+\mathbf{G},\omega) = \gamma_{LL'}(\mathbf{q},\omega)$. With these notations, the LDA spin susceptibility [Eq. (1)] takes the following form:

$$\chi_{\mathbf{G},\mathbf{G}'}^{(0)}(\mathbf{q},\omega) = \sum_{LL'} F_L^*(\mathbf{q}+\mathbf{G}) \gamma_{LL'}(\mathbf{q},\omega) F_{L'}(\mathbf{q}+\mathbf{G}'). \quad (10)$$

It is apparent from Eqs. (2), (9), and (10), that the computation of three types of quantities is required in a wide range of $\mathbf{q}$, $\mathbf{k}$, and ω: These are the multiband matrix $\gamma_{\eta'\eta}$ the matrix elements $A_L^{\eta'\eta}$, and the form factor F_L.

For an analysis of inelastic neutron scattering as a function of momentum $\hbar(\mathbf{q}+\mathbf{G}) = \hbar\mathbf{Q}$ and energy $\hbar\omega$ transfer, the diagonal $(\mathbf{G}'=\mathbf{G})$ term $\chi_{\mathbf{G},\mathbf{G}}(\mathbf{q},\omega) = \chi(\mathbf{Q},\omega)$ should be calculated including the relevant electron interactions. This will be discussed in the next section. At this stage, we calculate first the unenhanced $\chi^{(0)}(\mathbf{Q},\omega)$. This is done along three high-symmetry directions ΓX, ΓK, and ΓL in reciprocal space, which are further abbreviated by X, K, and L, respectively. For each of these directions D, wave vectors $\mathbf{q}$ and $\mathbf{G}$ are parallel and the use of a modulus Q^D of the wave vector $\mathbf{Q} = \mathbf{q}+\mathbf{G}$ is sufficient, provided the system has space inversion symmetry.

In the static $(\omega=0)$ limit, the spin susceptibility $\chi^{(0)}(\mathbf{Q},0)$ is calculated, and the results are displayed in Fig. 2 as a set of functions $\chi_D^{(0)}(Q)$ with wave vectors of length Q along the directions $D=X, K, L$. For $Q>2a^*$, the suscepti-

bility is considerably suppressed due to the form factor.

One notices a significant variation of $\chi_D^{(0)}(Q)$ over the whole range of the wave vectors chosen. Since we intent to apply the RPA theory, the positions of the maxima in $\mathbf{Q}$ space of the unenhanced susceptibility $\chi^{(0)}(\mathbf{Q},0)$ provide a valuable information: At these wave vectors and in their vicinity, one expects the strongest spin correlations when the enhanced $\chi(\mathbf{Q},0)$ is calculated.

For each direction D, two maxima of $\chi_D^{(0)}(Q)$ at wave vectors Q_{c1}^D and Q_{c2}^D are found; the second strongly suppressed maximum at $Q_{c2}^L>2a^*$ along the L-direction is not depicted here. The maxima at smaller Q_{c1}^D $(<Q_{c2}^D)$ are located in the first cubic BZ, while those at Q_{c2}^D are in the next BZ.

From now on, let us refer to the three wave vectors $Q_c = Q_{c1}^{X,K,L}$ as the "critical" ones. From Fig. 2, we obtain the following estimates: $Q_{c1}^X \approx 0.50$ Å^{-1}, $Q_{c1}^K \approx 0.65$ Å^{-1}, and $Q_{c1}^L \approx 0.75$ Å^{-1}. Remarkably, these three values occur within the range 0.4 Å$^{-1} \lesssim Q \lesssim 0.8$ Å^{-1}, where the main quasielastic neutron scattering is observed.[8–10]

The frequency distribution of spin fluctuations of the system of independent electrons may be seen from Fig. 3, where representative results of the calculated $\mathrm{Im}\,\chi_D^{(0)}(\mathbf{Q},\omega)$ are shown for three wave vectors of different lengths chosen along each of the high-symmetry directions D. For instance, at small wave vectors Q along the L direction, $\mathrm{Im}\,\chi_L^{(0)}(Q,\omega)$ shows a low-ω single-peaked structure. With increasing values of Q, the low-ω peak moves upward, and an additional broad distribution arises and grows gradually at higher frequencies. At the critical wave vector Q_{c1}^L, the pronounced low-ω peak at $\hbar\omega \sim 0.2$ eV still survives. However, a large portion of the spectral weight is found now within a broad distribution over much higher frequencies. As Q grows further, the low-ω peaked feature gets suppressed, and most of the spectral weight is shifted to the high-frequency region. As long as considerable spectral weight of the low-ω peaked feature of $\mathrm{Im}\,\chi_L^{(0)}(Q,\omega)$ is present, like at $Q \approx Q_{c1}^L$, its position on the ω axis is regarded as a bare (unrenormalized) spin relaxation rate $\Gamma^{(0)}(Q)$ characteristic of low-ω spin fluctuations. As expected, bare values of $\Gamma^{(0)}(Q)$, for instance, $\Gamma^{(0)}(Q_{c1}^L) \approx 0.2$ eV, are much too high to explain the slow spin dynamics found in the experiment.[8–10] Similar arguments are also applicable to the behavior of $\mathrm{Im}\,\chi_D^{(0)}(Q,\omega)$ along K and X directions displayed in Fig. 3. Therefore, interactions between quasiparticles must play an essential role to reach the observed energy scale Γ of spin fluctuations. In the next section, interaction effects are taken into account in the form of RPA theory.

III. RANDOM-PHASE APPROXIMATION APPROACH TO THE DYNAMIC SPIN SUSCEPTIBILITY OF LiV$_2$O$_4$

Within linear response theory, the time-Fourier transform of the dynamic spin susceptibility obeys the following integral equation:

$$\chi(\mathbf{r},\mathbf{r}';\omega) = \chi^{(0)}(\mathbf{r},\mathbf{r}';\omega) + \int d\mathbf{r}'' \chi^{(0)}$$

$$\times (\mathbf{r},\mathbf{r}'';\omega)\mathcal{K}(\mathbf{r}'')\chi(\mathbf{r}'',\mathbf{r}';\omega). \quad (11)$$

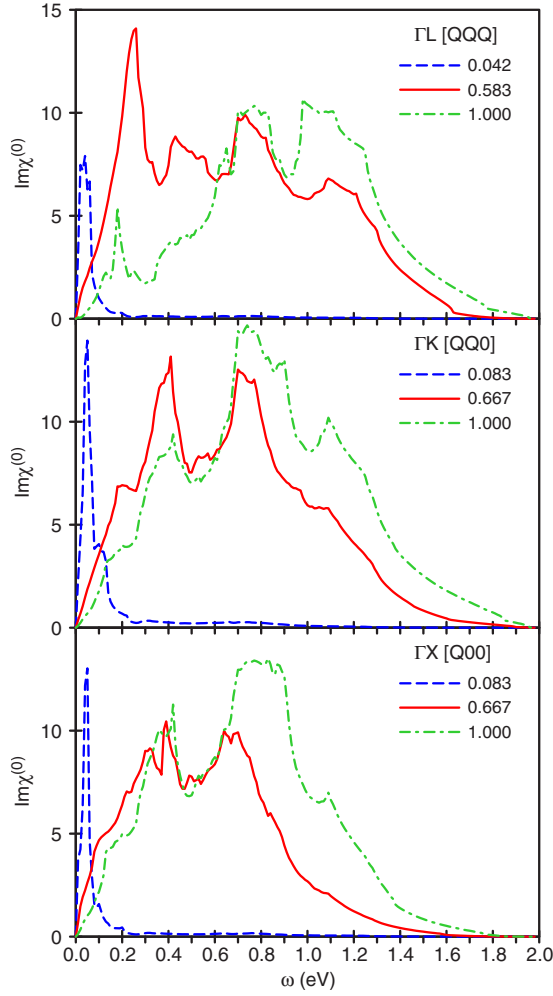Here, $\mathcal{K}(\mathbf{r})$ is a first derivative of the spin-dependent part of

FIG. 3. (Color online) Unenhanced Im $\chi^{(0)}(\mathbf{Q}, \omega)$ calculated at three different wave vectors chosen along the high-symmetry directions $D = L, K, X$. The critical wave vectors $Q_{c1}^{L,K,X}$ are denoted by the Cartesian component lengths 0.583, 0.667, and 0.667 (in units of $a^\star$), respectively.

the exchange-correlation potential V_{xc}^s taken in the local approximation. Since $\mathcal{K}(\mathbf{r})$ is a periodic function, $\mathcal{K}(\mathbf{r}+\mathbf{j}) = \mathcal{K}(\mathbf{r})$, its reciprocal-space counterpart $\mathcal{K}(\mathbf{G})$ is a function of the reciprocal-lattice vectors $\mathbf{G}$. After performing the double space-Fourier transformation, Eq. (11) is expressed as

$$\chi_{\mathbf{GG'}}(\mathbf{q}, \omega) = \chi_{\mathbf{GG'}}^{(0)}(\mathbf{q}, \omega) + \sum_{\mathbf{G}_1 \mathbf{G}_1'} \chi_{\mathbf{GG}_1}^{(0)}(\mathbf{q}, \omega) \mathcal{K}_{\mathbf{G}_1 \mathbf{G}_1'} \chi_{\mathbf{G}_1' \mathbf{G}'}(\mathbf{q}, \omega),$$

(12)

with $\mathcal{K}_{\mathbf{G}_1 \mathbf{G}_1'} = \mathcal{K}(\mathbf{G}_1 - \mathbf{G}_1')$. Solving Eq. (12) requires an inversion of an infinite matrix $(1 - \chi^{(0)} \mathcal{K})_{\mathbf{GG'}}$ in reciprocal-lattice (**G**) representation. To tackle the problem, first, one has to examine the convergence of the matrix elements of the susceptibility as the dimension of the (**G**)-basis increases. To avoid this, we use below a procedure suggested and developed in Refs. 21 and 28.

The separable form [Eq. (10)] of $\chi^{(0)} = F^* \gamma F$ allows us to solve the matrix inversion problem by transforming it from

G representation to the orbital L representation. Actually, the iteration procedure applied to Eq. (12) yields the matrix expansion $\chi = F^* \gamma (1 + M + M^2 + \cdots) F$, where the matrix elements of M are

$$M_{L_1 L_3}(\mathbf{q}, \omega) = \sum_{L_2} \left[\sum_{\mathbf{GG'}} F_{L_1}(\mathbf{q}+\mathbf{G}) \mathcal{K}_{\mathbf{GG'}} F_{L_2}^*(\mathbf{q}+\mathbf{G'}) \right]$$
$$\times \gamma_{L_2 L_3}(\mathbf{q}, \omega).$$

(13)

Assuming a convergence of the above power series of M at any $\mathbf{q}$ and ω, it can be converted into a familiar form $[1 - M]^{-1}$. Before doing this, let us consider the matrix elements $[\Sigma F \mathcal{K} F^*]_{L_1 L_2}$ entering the definition [Eq. (13)] of the matrix M and specify its indices as $L_1 = (\tau_1 m_1')(\tau_1 m_1)$ and $L_2 = (\tau_2 m_2')(\tau_2 m_2)$. Then, by using the definition [Eq. (8)] for the approximate form factor F and the inverse Fourier transformation for $\mathcal{K}$, a matrix element $[\Sigma F \mathcal{K} F^*]_{L_1 L_2}$ can be presented as a space integral of a product function of $\mathcal{K}(\mathbf{r})$ and two pairs of localized orbitals $w_m(\mathbf{r}-\mathbf{j}-\boldsymbol{\tau})$. In general, there are one-center and two-center integrals. We neglect interactions between different sites and retain only the one-center integrals. Thus, we use the approximation

$$\left[\sum_{\mathbf{GG'}} F(\mathbf{q}+\mathbf{G}) \mathcal{K}_{\mathbf{GG'}} F^*(\mathbf{q}+\mathbf{G'}) \right]_{L_1 L_2} \simeq \delta_{\tau_1 \tau_2} \mathcal{K}(m_1' m_1; m_2' m_2),$$

$$\mathcal{K}(m_1' m_1; m_2' m_2) = v_0 \int_{v_0} d\mathbf{r} \, w_{m_1'}(\mathbf{r}) w_{m_1}(\mathbf{r}) \mathcal{K}(\mathbf{r}) w_{m_2'}(\mathbf{r}) w_{m_2}(\mathbf{r}).$$

(14)

Furthermore, we keep only the diagonal matrix elements $\mathcal{K}(m, m; m, m)$ which are assumed to be independent on m. Thus, the unique coupling constant $\mathcal{K}$ is the only adjustable parameter in our approximate approach. Finally, we arrive at the following expression for the enhanced spin susceptibility:

$$\chi_{\mathbf{G}, \mathbf{G'}}(\mathbf{q}, \omega) = \sum_{LL'L''} F_L^*(\mathbf{q}+\mathbf{G}) \gamma_{LL''}(\mathbf{q}, \omega) \{[1$$
$$- \mathcal{K}\gamma(\mathbf{q}, \omega)]^{-1}\}_{L''L'} F_{L'}(\mathbf{q}+\mathbf{G'}),$$

(15)

where the elements of the matrix $\gamma(\mathbf{q}, \omega)$ are given by Eq. (9). The essence of the procedure is instead of inverting the large matrix needed to solve Eq. (12) to invert the smaller matrix $(1 - \chi^{(0)} \mathcal{K})_{LL'}$ in the orbital basis.

Because of the composite character of orbital indices L, matrix operations in L representation require additional comments. In particular, matrix elements of a transposed matrix $\tilde{\gamma}$ are related to those of the direct matrix as $\tilde{\gamma}_{L_1 L_2} = \gamma_{\bar{L}_2 \bar{L}_1}$, where each composite index $L_n = (\tau_n' m_n')(\tau_n m_n)$ is also transposed to give $\bar{L}_n = (\tau_n m_n)(\tau_n' m_n')$. Therefore, for a Hermitian conjugate matrix $\gamma^\dagger$, one has $\gamma_{L_1 L_2}^\dagger = \gamma_{\bar{L}_2 \bar{L}_1}^*$. There are 144 distinct indices L; therefore, γ is a (144×144) matrix. The large number of elements $\gamma_{LL'}(\mathbf{q}, \omega)$ that have to be determined for each value of $\mathbf{q}$ and ω makes the numerical calculations of χ a rather complicated problem. At some stage pointed out below, we will introduce a simplification ("diagonal" approximation for the matrix γ) allowing us to reduce

the matrix dimensionality and, thus, make a numerical analysis feasible.

According to definition (9), the matrix $\gamma(\mathbf{q}, \omega)$ can be generally decomposed as follows:

$$\gamma(\mathbf{q}, \omega) = \gamma^{(1)}(\mathbf{q}, \omega) + i\gamma^{(2)}(\mathbf{q}, \omega). \qquad (16)$$

Here, the elements of the Hermitian matrix $\gamma^{(1)} = (\gamma + \gamma^\dagger)/2$ are even functions of ω, while those of the anti-Hermitian matrix $\gamma^{(2)} = (\gamma - \gamma^\dagger)/2i$ are odd functions of ω. Note that $\gamma^{(2)}(\mathbf{q}, 0) = 0$ for all $\mathbf{q}$.

Let us consider the static, $\omega = 0$, limit and solve the eigenvalue problem for the Hermitian matrix $\gamma(\mathbf{q}, 0) = \gamma^{(1)}(\mathbf{q}, 0)$:

$$\sum_{L'} \gamma_{LL'}(\mathbf{q}, 0) V_{L'}^{(k)}(\mathbf{q}) = \lambda^{(k)}(\mathbf{q}) V_L^{(k)}(\mathbf{q}), \qquad (17)$$

where $V_L^{(k)}$ are components of the kth eigenvector with the eigenvalue $\lambda^{(k)}$. The static spin susceptibility takes the following form:

$$\chi_{\mathbf{G}, \mathbf{G}}(\mathbf{q}, 0) = \sum_k |\mathcal{F}^{(k)}(\mathbf{q}, \mathbf{G})|^2 \frac{\lambda^{(k)}(\mathbf{q})}{1 - \mathcal{K}\lambda^{(k)}(\mathbf{q})}, \qquad (18)$$

with $\mathcal{F}^{(k)}(\mathbf{q}, \mathbf{G}) = \Sigma_L F_L^*(\mathbf{q} + G) V_L^{(k)}(\mathbf{q})$. In solving Eq. (17), we adopt a diagonal approximation[21] which consists in retaining in $\gamma_{LL'}$ only the diagonal composite indices, $L = (\tau m)(\tau m)$ and $L' = (\tau' m')(\tau' m')$. Then, $\gamma_{LL'}$ becomes a (12×12) matrix. A partial justification is that the moduli of the off-diagonal, $(\tau' m') \neq (\tau m)$, matrix elements [Eq. (7)] are small in our calculations. To assess the accuracy of the diagonal approximation, a small set of arbitrary wave vectors $\mathbf{q}$ was chosen, and Im $\chi^{(0)}(\mathbf{q}, \omega)$ was calculated (at $\mathbf{G} = \mathbf{G}' = 0$) as a function of ω including either all or only diagonal elements of the matrix γ. At each $\mathbf{q}$ probed, we found rather tiny differences between the two curves.

Like in Sec. II, we consider below only the high-symmetry X, K, and L directions in reciprocal space. For each direction D, let us pick out the critical wavevector Q_c^D and rearrange the set of $\lambda^{(k)}(Q_c^D) = \lambda_D^{(k)}$ in the following order: $\lambda_D^{(1)} > \lambda_D^{(2)} > \lambda_D^{(3)} > \cdots$. For brevity, a set of nondegenerate $\lambda_D^{(k)}$ is discussed here. The first members of the set $\lambda_D^{(k)}$ at $k = 1, 2, \ldots$, are positive in order to ensure $\chi_{\mathbf{G}, \mathbf{G}}(\mathbf{q}, 0) > 0$, provided $\mathcal{K}$ is below some critical value $\mathcal{K}_c$. It is apparent from Eq. (18) that along the D direction, the $\lambda_D^{(1)}$ mode is the most critical one in the sense that $0 \leq 1 - \mathcal{K}\lambda_D^{(1)} < 1 - \mathcal{K}\lambda_D^{(2)} < 1 - \mathcal{K}\lambda_D^{(3)} < \cdots$. A magnetic instability occurs if the condition $1 - \mathcal{K}\lambda_D^{(1)} = 0$ is fulfilled. This defines $\mathcal{K}_c$. Among the three directions under consideration, the smallest $\mathcal{K}_c = 0.49$ eV occurs along the L direction at $Q_{c1}^L \approx 0.75$ Å^{-1}. Since for X and K directions the instability conditions are fulfilled at values of $\mathcal{K}$ that are close but somewhat larger than $\mathcal{K}_c = 0.49$ eV, the latter value is chosen to be the best estimate of the critical value of the exchange-correlation parameter $\mathcal{K}$. In LiV$_2$O$_4$, spin dynamics of a magnetically disordered state with strongly enhanced spin fluctuations may be described by Eq. (15) with the parameter $\mathcal{K}$ approaching $\mathcal{K}_c$ from below.

The enhancement of the static susceptibility [Eq. (18)] in a spin disordered state is controlled by a generalized Stoner factor $S_\mathcal{K}(\mathbf{Q}) = [1 - \mathcal{K}\lambda^{(1)}(\mathbf{Q})]^{-1}$, which is a function of both
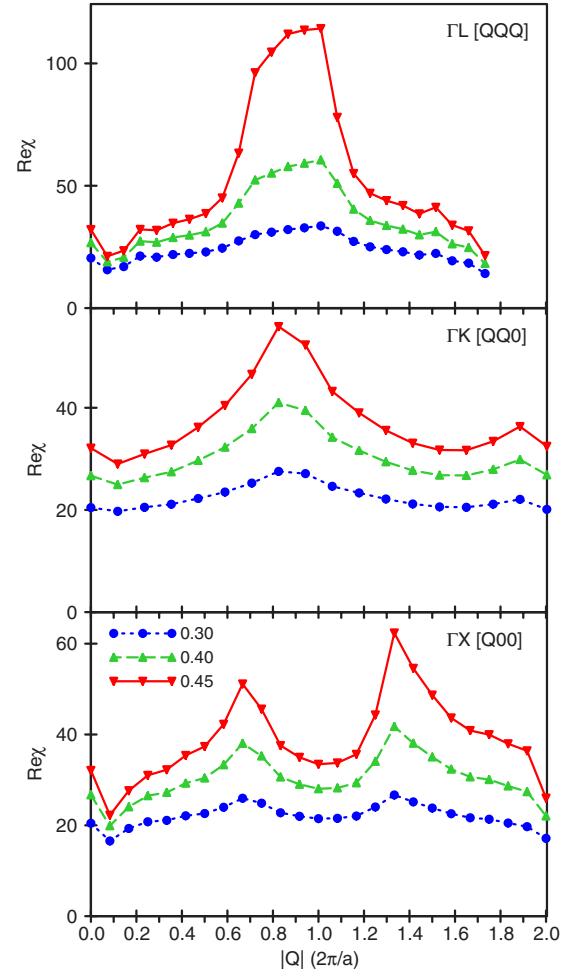

FIG. 4. (Color online) Evolution of the static spin susceptibility $\chi(\mathbf{Q}, 0)$ for different values of the coupling constant $\mathcal{K} \to \mathcal{K}_c = 0.49$ eV. Representative values of $\mathcal{K}$ (in eV) chosen are shown in the bottom panel.

$\mathcal{K}$ and $\mathbf{Q}$, with the obvious property $S_\mathcal{K}(Q_{c1}^L) \to \infty$ as $\mathcal{K} \to \mathcal{K}_c$. Thus, the Stoner factor describes the proximity of the system to the instability. As may be seen from Fig. 4, the strongest enhancement of the static susceptibility [Eq. (18)] is found for spin fluctuations at and nearby the critical wave vectors Q_c and at Q_{c2}^X. At the same time, the Stoner factor is of a moderate size for the remaining wave vectors.

Very similar Q dependence of the exchange-correlation effects is seen from the calculated imaginary part of the enhanced dynamic spin susceptibility Im $\chi_D(Q, \omega)$.

Results for the calculated Im $\chi_D(Q, \omega)$ are shown in Fig. 5. They have to be compared with the unenhanced spin susceptibility Im $\chi_D^{(0)}(Q, \omega)$ plotted in Fig. 3. Let us follow the evolution of the ω dependence of Im $\chi_L(Q, \omega)$ along the L direction with increasing $\mathcal{K} \to \mathcal{K}_c$. Like in Fig. 3, three characteristic wave vectors are chosen to distinguish the behavior at critical $Q^L \simeq Q_{c1}^L$ from those at smaller and larger wave vectors. As expected, the net frequency dependence of Im $\chi_L(Q, \omega)$ is most strongly affected at Q_{c1}^L. In the upper panel of Fig. 5, a large portion of the spectral weight is transferred to the low-energy region, though at Q_{c1}^L, the overall spectral distribution still extends up to ~ 2 eV. The pro-
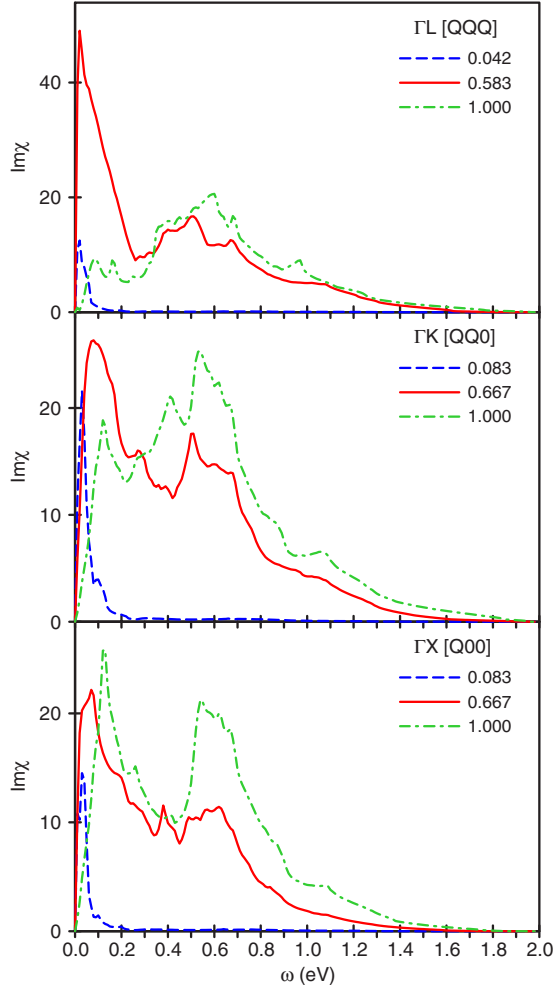
FIG. 5. (Color online) Enhanced Im $\chi(\mathbf{Q},\omega)$ calculated at $\mathcal{K}$ $=0.95\mathcal{K}_c$ for the same wave vectors as in Fig. 3. Note that the size along the vertical axis is amplified to that in Fig. 3.

nounced low-ω feature seen at Q_{c1}^L strongly dominates those at smaller and larger wave vectors.

Generally, in the low-ω limit, the imaginary part of $\chi(Q,\omega)$ can be accurately approximated by

$$\text{Im } \chi(Q,\omega) \simeq z_Q \chi(Q)\omega/\Gamma(Q), \qquad (19)$$

where the weight factor $z_Q < 1$. Again, by choosing the L direction as the most representative one, we have compared the initial gradients of several curves representing Im $\chi_L(Q_{c1},\omega)$ for different $\mathcal{K} \lesssim \mathcal{K}_c$ and found that the initial slope is proportional to $S_{\mathcal{K}}^2(Q_{c1}^L)$ and thus grows very fast as $\mathcal{K} \to \mathcal{K}_c$. The factor $S_{\mathcal{K}}^2(Q)$ stems from the Stoner enhanced static susceptibility, $\chi(Q) \simeq S_{\mathcal{K}}(Q)\chi^{(0)}(Q)$, and a renormalization of the spin relaxation rate, $\Gamma(Q) \simeq \Gamma^{(0)}(Q)/S_{\mathcal{K}}(Q)$. Far away from Q_{c1}^L, the same relation holds, however, with much weaker enhancement factor, $S_{\mathcal{K}}^2(Q^L) \ll S_{\mathcal{K}}^2(Q_{c1}^L)$. Concerning the evolution of Im $\chi_D(Q,\omega)$ for $D=X, K$ with increasing $\mathcal{K}$, our calculations show a similar behavior, i.e., strongly enhanced spin fluctuations at $Q^D \sim Q_c^D$ in the low-ω region.

If the value of the adjustable coupling parameter $\mathcal{K}$ is tuned close to $\mathcal{K}_c$, then $\Gamma(Q_c)$ may be reduced to values as

low as the experimentally observed ones. However, this should not be taken as a literal explanation of experimental data because close to the critical condition, RPA becomes less reliable. Furthermore, in our approach, we ignored the quantitative contribution of intersite charge correlations to the reduction of $\Gamma^{(0)}$. Instead, our purpose is to show that like in many other materials, in the case of LiV_2O_4, the RPA theory is a useful tool in taking into account the qualitative effects of strong electron correlations, which provide a basic mechanism for a strong reduction of spin relaxation rate in a broad region of $\mathbf{Q}$ space.

To complete our analysis, it is tempting to associate the coupling parameter $\mathcal{K}$ with the exchange-correlation integral I (i.e., the local Stoner parameter) calculated within the local spin-density approximation (LSDA) at $T=0$. The corresponding procedure was suggested and discussed in Refs. [29–32]. We performed calculations for LiV_2O_4 with the Perdew-Wang form for the exchange-correlation potential and found $I=0.65$ eV. Assuming this estimate as the bare value of the coupling $\mathcal{K}_0=I$ and taking the paramagnetic static susceptibility $\chi^{(0)}(\mathbf{Q})$ calculated at $T=0$, we obtain $\mathcal{K}_0\chi^{(0)}(\mathbf{Q}) > 1$ both for $\mathbf{Q}=0$ and $\mathbf{Q}=\mathbf{Q}_c$. This implies an unstable paramagnetic state in LiV_2O_4 at $T=0$. The instability of a paramagnetic state obtained in LSDA calculations for LiV_2O_4 was also reported in Refs. [13] and [14]. At first sight, this observation is in conflict with the assumptions of a paramagnetic ground state.

However, the following arguments show that the actual value of the coupling parameter $\mathcal{K}$ is smaller than the bare value $\mathcal{K}_0$ and may be well below the critical value $\mathcal{K}_c$ because of possible strong renormalization due to zero-point spin fluctuations. Actually, because we apply LSDA theory, the calculated exchange-correlation integral I has to be considered as a mean-field value. The self-consistent renormalization (SCR) theory[33,34] of spin fluctuations in nearly ferro-or antiferromagnetic metals modifies the condition for a magnetic instability with respect to the mean-field prediction. At $T=0$, the main effect of the SCR correction to the RPA spin susceptibility is a reduction of a bare, mean-field coupling parameter entering the Stoner enhancement factor. In our notation, this reads as

$$\mathcal{K} = \mathcal{K}_0 - |F_Q|\sum_\alpha (m_\alpha^2)_0. \qquad (20)$$

Here, $|F_Q|$ is the mode-mode coupling constant for dominant spin fluctuations at $Q \approx Q_c$, and $(m_\alpha^2)_0$ is the mean square local amplitude of the spin fluctuations at $T=0$:

$$(m_\alpha^2)_0 = \frac{1}{2\pi}\int_0^\infty d\omega \frac{1}{N}\sum_{\mathbf{q}} \text{Im } \chi(\mathbf{q},\omega). \qquad (21)$$

The exact dynamic spin susceptibility in Eq. (21) can be replaced approximately by the RPA expression with the actual coupling parameter $\mathcal{K}$. Thus, Eqs. (20) and (21) lead to a complicated equation for $\mathcal{K}$. As $|F_Q|$ is still unknown, we cannot give a quantitative estimate for $\mathcal{K}$ from the equation obtained and restrict ourselves to the following remark on its property: Provided a large region of $\mathbf{q}$ space is occupied with well developed and enhanced spin fluctuations, the mean-
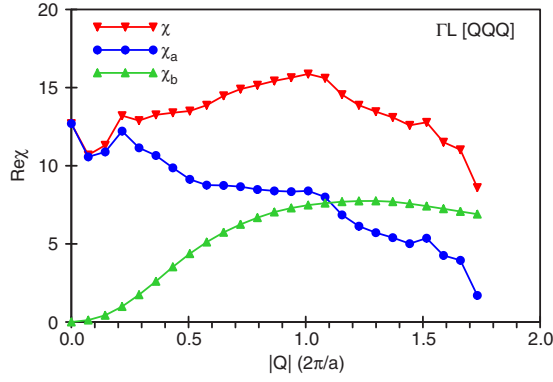
FIG. 6. (Color online) Two contributions $\chi_a^{(0)}(\mathbf{Q})$ and $\chi_b^{(0)}(\mathbf{Q})$ (see text) to the unenhanced static spin susceptibility $\chi^{(0)}(\mathbf{Q})$ calculated along the L direction.

field coupling $\mathcal{K}_0 > \mathcal{K}_c$ is reduced to a value below $\mathcal{K}_c$. The distribution in $\mathbf{q}$ space of enhanced low-ω spin fluctuations is discussed in the next section. These fluctuations contribute considerably to the renormalization of the coupling constant. Whether the resulting value of $\mathcal{K}$ occurs near the critical $\mathcal{K}_c$ depends on the energy parameter $|F_Q|$ that can now be regarded as the only adjustable parameter of the theory.

Now, we discuss to which extent geometrical frustration inherent in the pyrochlore lattice can influence magnetic properties of itinerant electron system.

The concept of frustration is primarily used for localized spin systems. In a given frustrated lattice, it means that the exchange energy of nearest neighbor (nn) antiferromagnetic bonds between local moments cannot be minimized simultaneously for each bond. On the other hand, for free electrons with nn hopping on the same lattice, there is no frustration in a similar sense. However, the "corner sharing tetrahedra" property of the pyrochlore lattice leads to flat energy bands for the electrons. This can be seen in the LDA bands in Fig. 1, where the topmost unoccupied bands derived from the t_{2g} vanadium orbitals have almost no dispersion. Next, we show that the spin susceptibility $\chi^{(0)}(\mathbf{Q})$ of LiV$_2$O$_4$ calculated in the limit of noninteracting electrons is strongly affected by these nearly flat bands. To this end, we divide the set of 12 bands, Fig. 1, into two subsets. The first contains the band states with energies below 0.4 eV, while the second subset is formed of the upper bands. To distinguish two kinds of particle-hole excitations, the dynamic spin susceptibility can be written now as $\chi^{(0)}(\mathbf{Q}, \omega) = \chi_a^{(0)}(\mathbf{Q}, \omega) + \chi_b^{(0)}(\mathbf{Q}, \omega)$. Both the intra- and interband electron transitions between band states from the first subset are allowed and contribute to $\chi_a^{(0)}$, while only interband transitions between occupied $\mathbf{k}$ states from the first subset to unoccupied $(\mathbf{k}+\mathbf{Q})$ states from the second subset contribute to $\chi_b^{(0)}$. With the use of the Kramers-Kronig relation, the static susceptibility $\chi^{(0)}(\mathbf{Q})$ $= \chi_a^{(0)}(\mathbf{Q}) + \chi_b^{(0)}(\mathbf{Q})$ is calculated and the results for the L direction is shown in Fig. 6. First, the contribution $\chi_a^{(0)}(\mathbf{Q})$ varies strongly with $\mathbf{Q}$ with the maximum at $\mathbf{Q}=0$ that strongly exceeds a value at the critical $\mathbf{Q}_c^L$. In contrast, for the second contribution, one has $\chi_b^{(0)}(0)=0$ because of the orthogonality condition given by Eq. (5) and a smooth behavior as a function of $\mathbf{Q}$, since for finite $\mathbf{Q}$, the wave func-

tions of different bands are no longer orthogonal. Because of this contribution, the dominant maximum of the total static susceptibility $\chi^{(0)}(\mathbf{Q})$ is shifted away from the BZ center to a critical wave vector $\mathbf{Q}_c^L$. Thus, for interacting electrons on the pyrochlore lattice, antiferromagnetic fluctuations are more preferable than ferromagnetic ones at least at $T=0$. The presence of a large one-particle density of states associated with nearly flat electronic bands not far from the Fermi energy explains this preference.

Another aspect of geometrical frustration is the suggested strong degeneracy (multiplicity) of critical wave vectors $\mathbf{Q}_c$. Expressed differently, the near $\mathbf{Q}$ independence of the susceptibility $\chi(\mathbf{Q})$ in a large sector of the BZ means that on approaching the critical interaction $\mathcal{K}_c$, the system cannot choose a unique wave vector of a magnetic structure which minimizes the free energy of spin fluctuations. Instead, it is frustrated between different structures with different wave vectors and equally low free energy.

IV. DISCUSSION

In this section we want to put our results in a more general context. Quasielastic neutron scattering studies of powder samples of LiV$_2$O$_4$ suggest that in the low-T limit and in a range of wave vectors, $0.4 \text{ Å}^{-1} \lesssim Q \lesssim 0.8 \text{ Å}^{-1}$, the vanadium spin system exhibits strongly enhanced and slow spin fluctuations. A complete theoretical analysis of these data would require calculations of the dynamic spin susceptibility in a wide range of $(\mathbf{Q}, \omega)$ space. In principle, that is possible within our approximation scheme except for the large computational time required. The calculation of $\chi(\mathbf{Q}, \omega)$ can be performed in any domain of $(\mathbf{Q}, \omega)$ space, not only along the high-symmetry $\mathbf{Q}$ directions. However, even the limited results of Secs. II and III provide a valuable and essential piece of information on the spin-fluctuation dynamics in LiV$_2$O$_4$.

Actually, a particular $\mathbf{Q}$ dependence of the calculated unenhanced spin susceptibility $\chi^{(0)}(\mathbf{Q}, 0)$, which involves the actual band structure of LiV$_2$O$_4$, clearly displays in Fig. 2 that the particular critical wave vectors $Q_{c1}^{X,K,L}$ are grouped in the range $0.5 \text{ Å}^{-1} \lesssim Q_c \lesssim 0.8 \text{ Å}^{-1}$, where the pronounced quasielastic neutron scattering is observed. However, the bare spin relaxation rate $\Gamma^{(0)}(Q) \sim 200$ meV is much too large to be compatible with experimental observations. This disagreement has to be attributed to strong electron correlations not included in LDA calculations. Taking them into account by means of a RPA, we have obtained an enhanced susceptibility $\chi(\mathbf{Q}, \omega)$ as is seen by comparing Figs. 3 and 5. As the coupling tends to the critical value, $\mathcal{K} \to \mathcal{K}_c$, spin fluctuations near Q_c are strongly renormalized: A large fraction of the spectral weight is shifted to low frequencies, thus resulting in an enhanced low-energy response.

Next, we want to discuss in more detail the part of $\mathbf{Q}$ space with slow spin fluctuations. The wave vectors $\mathbf{Q}_c$ $=\mathbf{Q}_{c1}^{X,K,Z}$ are positioned on a smooth three dimensional surface to which we refer as critical $\mathbf{q}_c$ surface. This surface is in the first cubic Brillouin zone, and we shall replace $\mathbf{Q}$ by $\mathbf{q}$ in that case. We have checked by additional calculations that spin fluctuations are slow everywhere on the $\mathbf{q}_c$ surface. Moreover, the broad maxima of $\chi(\mathbf{q}, 0)$ in Fig. 4 suggest that
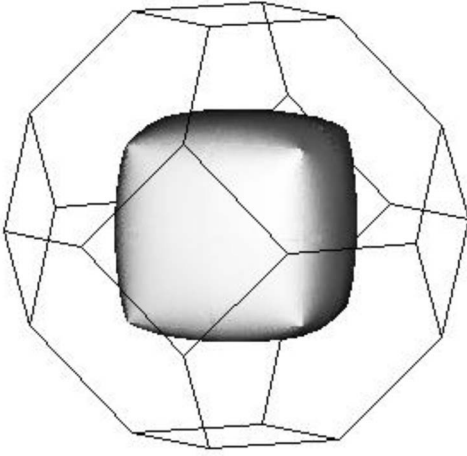
FIG. 7. A surface in **Q** space representing the lower bound for the critical region of strongly enhanced slow spin fluctuations. The upper bound is the larger congruent surface at a distance $|\delta\mathbf{Q}| \simeq 0.3a^\star$ from the smaller one shown.

the region of slow fluctuations extends over a width of $(|\mathbf{q}_c| - \delta q/2) < |\mathbf{q}| < (|\mathbf{q}_c| + \delta q/2)$, while the $\mathbf{q}_c$ surface lies midway between two bounds. The lower bound of this region is shown by the surface depicted in Fig. 7. It intersects the X axis (and the equivalent Y and Z axes) at $(q_{c1}^X - \delta q/2) \approx 0.5a^\star \approx 0.4$ Å$^{-1} \equiv q_1^X$. The upper bound is a congruent surface crossing the X axis at $(q_{c1}^X + \delta q/2) \approx 0.8a^\star \approx 0.6$ Å$^{-1} \equiv q_2^X$. Thus, q_1^X and q_2^X are minimal radii of two bounds. The width δq is estimated to be $\delta q \approx 0.3a^\star \lesssim 0.23$ Å^{-1}. Multiplicity of critical wave vectors distributed over an extended region in **q** space is a consequence of geometrical frustration in the pyrochlore lattice.

The suggested distribution in **q** space of strongly enhanced and slow spin fluctuations is compatible with the angular averaged data derived from inelastic neutron scattering on polycrystalline samples.[8–10] Indeed, as seen from Fig. 4, the next pronounced maximum of $\chi(\mathbf{Q}, 0)$ is found along the X direction at $Q_{c2}^X \approx 1.4a^\star \approx 1$ Å^{-1}. Together with the other equivalent directions, it makes up a six-point manifold, but their partners at $Q_{c2}^{K,L}$ are strongly suppressed by the form factor. Therefore, this secondary manifold is not resolved in the experiment.

Many metallic systems with enhanced spin fluctuations show dramatically renormalized thermodynamic properties, for instance, a tendency to the formation of heavy-fermion properties: a strongly enhanced linear term γT of the specific heat and a concomitantly enhanced magnetic susceptibility χ. In many $4f$- and $5f$-derived heavy-fermion systems, the spin fluctuations are soft (have low ω) over the large portion of the reciprocal space, which provides a large value of γ. A different case is the nearly antiferromagnetic metal $Cr_{0.95}V_{0.05}$, which is close to incommensurate magnetic order. In contrast to the heavy-fermion systems, $Cr_{0.95}V_{0.05}$ has a typical, unenhanced value of the measured γ, which is explained[35] to be due to the small region in the momentum space occupied by the exchange enhanced soft spin fluctuations in this material.

It is promising now to develop a spin-fluctuation theory for LiV_2O_4 and estimate the contribution of spin fluctuations

to the low-T specific heat. The theory is aimed at an approximate description of the low-ω behavior of the calculated $\chi(\mathbf{q}, \omega)$ in terms of overdamped oscillators. One has to start with the following definition of the spin-fluctuation free energy[24–26]:

$$F_{sf} = \frac{3}{\pi} \sum_{\mathbf{q}} \int_0^{\omega_c} d\omega F_{osc}(\omega) \frac{z(\mathbf{q})\Gamma(\mathbf{q})}{\omega^2 + \Gamma^2(\mathbf{q})}, \qquad (22)$$

where $F_{osc}(\omega) = k_B T \ln[1 - \exp(-\hbar\omega/k_B T)]$ is the thermal part of the free energy of an oscillator, $z(\mathbf{q})$ is the spectral weight of a low-ω spin-fluctuation mode, and ω_c is the cutoff frequency. The specific heat is given by $C_{sf}(T) = (-T/N) \times (\partial^2 F_{sf}/\partial T^2)$, where N is the number of V atoms in the system. In the limit $T \rightarrow 0$, simple calculation leads to the familiar expression for the spin-fluctuation contribution $\gamma_{sf} = C_{sf}(T)/T$ to the specific heat coefficient γ:

$$\gamma_{sf} = \frac{k_B^2 \pi}{N} \sum_{\mathbf{q}} \frac{z(\mathbf{q})}{\hbar\Gamma(\mathbf{q})}, \qquad (23)$$

where the summation is over the cubic BZ.

Our aim now is to propose a reliable simple model describing variations of $z(\mathbf{q})$ and $\Gamma(\mathbf{q})$ in **q** space. The model adopts the most essential low-ω properties of $\chi(\mathbf{q}, \omega)$ calculated for LiV_2O_4. We start by partitioning the **q** space into three regions: (I) the interior of the surface depicted in Fig. 7, i.e., $|\mathbf{q}| < (|\mathbf{q}_c| - \delta q/2)$, (II) the critical region $(|\mathbf{q}_c| - \delta q/2) < |\mathbf{q}| < (|\mathbf{q}_c| + \delta q/2)$, and (III) the periphery, $|\mathbf{q}| > (|\mathbf{q}_c| + \delta q/2)$, of the cubic BZ. Within layer (II), we approximate $\Gamma(\mathbf{q})$ and $z(\mathbf{q})$ by constants Γ and $z_{II} < 1$, respectively. Then, in region (I), $\Gamma_I(\mathbf{q}) = (q/q_1)\Gamma$ and $z_I(\mathbf{q}) = 1 - (1 - z_{II})q/q_1$, which provides a piecewise continuity between regions (I) and (II). Here, $q_1 \simeq 0.5a^\star$ and $q_2 \simeq 0.8a^\star$ are minimal radii of the lower (Fig. 7) and the upper bound surfaces for the critical region. Finally, as suggested from the analysis of Im $\chi(\mathbf{q}, \omega)$ at large **q**, in (III), the weight $z(\mathbf{q})$ decreases fast to zero. Therefore, this contribution is neglected below. After performing the integration in Eq. (23), we arrive at the following expression:

$$\gamma_{sf} = \frac{\pi^2}{32} k_B^2 \left[\left(\frac{q_1}{a^\star} \right)^3 + 2z_{II} \left(\frac{q_2}{a^\star} \right)^3 \right] \frac{1}{\hbar\Gamma}. \qquad (24)$$

In Eq. (24) an additional factor 1.5 takes into account a deviation of the critical surface shape from a spherical one.

An analysis of the calculated Im $\chi(\mathbf{q}, \omega)$ leads us to a rather rough estimate $z_{II} \approx 1/4$, while the reported[8–10] low-T values of $\hbar\Gamma$ in the critical region of **q** fall within the limits of 0.5 meV $< \hbar\Gamma < 5$ meV. By substituting these parameters into Eq. (24) and recalling that there are two V atoms in the formula unit, we obtain the estimate for γ_{sf} as $300 > \gamma_{sf} > 30$ in units of mJ/K^2 mol. This estimate shows that slow spin fluctuations over an extended region in **q** space may explain the size of the enhanced specific heat coefficient in LiV_2O_4.

It is instructive to estimate the Sommerfeld-Wilson ratio $R_W = \pi^2 k_B^2 \chi_S(T=0)/(3\mu_B^2 \gamma)$, where μ_B is the Bohr magneton. Taking the upper bound for γ coefficient as $\gamma \simeq 300$ mJ/K^2 mol and the value $\chi_S(T=0) = \chi(0,0)$ calculated

for $\mathcal{K}=0.95\mathcal{K}_c$ in our theory, one obtains $R_W \approx 5$. This result is in a contrast with the estimate $R_W \sim 0.1$ obtained within the RPA theory,[27] where both spin and orbital critical fluctuations were assumed to contribute.

V. CONCLUSIONS

The enhanced dynamic spin susceptibility of the multiband paramagnetic spinel LiV_2O_4 was calculated on the basis of the actual LDA band structure of this metallic system. It was shown that the complexity of the band structure results in an unenhanced spin susceptibility that displays a key information about spin fluctuations in this material, namely, the position in **Q** space of dominant spin correlations. The calculated moduli of these critical wave vectors $\mathbf{Q}_c$ located (at $T=0$) obviously far away from the Brillouin zone center are in a good agreement with experiment.

The susceptibility enhancement due to electron interaction is described and calculated in the RPA approach adopted to the actual multiband system with nearly degenerate d orbitals. The most substantial approximation we made is the neglect of the orbital dependence and the off-diagonal matrix elements of the matrix $\mathcal{K}$ defined by Eq. (14). A wave-vector dependence of $\mathcal{K}$ is also omitted, which, we believe, is less crucial since the vanadium d orbitals are well localized and strong on-site electronic correlations dominate. The approach developed above may be extended in the following ways. Provided a particular model of electron interaction is chosen and parametrized suitably, matrix elements of the $\mathcal{K}$ matrix entering expression (15) may be evaluated.[36] The resulting few-parameter theory then can be put on a quantitative ground by comparing the calculated model results with available experimental data.

Despite the approximations used in the description of electron correlations in a multiband electronic system such as LiV_2O_4, we believe that the approach developed here enabled us to catch, in accord with experimental observations, the most essential effect of correlations: enormous magnification and slowing down of spin fluctuations at critical wave vectors $\mathbf{Q}_c$.

[1] S. Kondo, D. C. Johnston, C. A. Swenson, F. Borsa, A. V. Mahajan, L. L. Miller, T. Gu, A. I. Goldman, M. B. Maple, D. A. Gajewski, E. J. Freeman, N. R. Dilley, R. P. Dickey, J. Merrin, K. Kojima, G. M. Luke, Y. J. Uemura, O. Chmaissem, and J. D. Jorgensen, Phys. Rev. Lett. **78**, 3729 (1997).

[2] D. Johnston, Physica B **281-282**, 21 (2000).

[3] S. Kondo, D. C. Johnston, and L. L. Miller, Phys. Rev. B **59**, 2609 (1999).

[4] N. Fujiwara, H. Yasuoka, and Y. Ueda, Phys. Rev. B **57**, 3539 (1998).

[5] K. Fujiwara, K. Miyoshi, J. Takeuchi, Y. Shimaoka, and T. Kobayashi, J. Phys.: Condens. Matter **16**, S615 (2004).

[6] A. Koda, R. Kadono, K. Ohishi, S. Saba, W. Higemoto, Y. Matsushita, and Y. Ueda, J. Phys.: Condens. Matter **17**, L257 (2005).

[7] A. Shimoyamada, S. Tsuda, K. Ishizaka, T. Kiss, T. Shimojima, T. Togashi, S. Watanabe, C. Q. Zhang, C. T. Chen, Y. Matsushita, H. Ueda, Y. Ueda, and S. Shin, Phys. Rev. Lett. **96**, 026403 (2006).

[8] A. Krimmel, A. Loidl, M. Klemm, S. Horn, and H. Schober, Phys. Rev. Lett. **82**, 2919 (1999).

[9] S. H. Lee, Y. Qiu, C. Broholm, Y. Ueda, and J. J. Rush, Phys. Rev. Lett. **86**, 5554 (2001).

[10] A. Murani, A. Krimmel, J. Stewart, M. Smith, P. Strobel, A. Loidl, and A. Ibarra-Palos, J. Phys.: Condens. Matter **16**, S607 (2004).

[11] P. Fulde, J. Phys.: Condens. Matter **16**, S591 (2004).

[12] J. Matsuno, A. Fujimori, and L. F. Mattheiss, Phys. Rev. B **60**, 1607 (1999).

[13] D. J. Singh, P. Blaha, K. Schwarz, and I. I. Mazin, Phys. Rev. B **60**, 16359 (1999).

[14] V. Eyert, K.-H. Höck, S. Horn, A. Loidl, and P. S. Riseborough, Europhys. Lett. **46**, 762 (1999).

[15] P. Fulde, A. Yaresko, A. Zvyagin, and Y. Grin, Europhys. Lett. **54**, 779 (2001).

[16] V. Yushankhai, P. Fulde, and P. Thalmeier, Phys. Rev. B **71**, 245108 (2005).

[17] T. Izuyama, D. Kim, and R. Kubo, J. Phys. Soc. Jpn. **18**, 1025 (1963).

[18] S. Doniach, Proc. Phys. Soc. London **91**, 86 (1967).

[19] J. Cooke, Phys. Rev. B **7**, 1108 (1973).

[20] J. Callaway and C. Wang, J. Phys. F: Met. Phys. **5**, 2119 (1975).

[21] J. Callaway, A. K. Chatterjee, S. P. Singhal, and A. Ziegler, Phys. Rev. B **28**, 3818 (1983).

[22] E. Stenzel and H. Winter, J. Phys. F: Met. Phys. **15**, 1571 (1985).

[23] E. Stenzel and H. Winter, J. Phys. F: Met. Phys. **16**, 1789 (1986).

[24] G. Lonzarich, J. Magn. Magn. Mater. **54-57**, 612 (1986).

[25] G. Lonzarich, N. Bernhoeft, and D. Paul, Physica B **156**, 699 (1989).

[26] R. Konno and T. Moriya, J. Phys. Soc. Jpn. **56**, 3270 (1987).

[27] Y. Yamashita and K. Ueda, Phys. Rev. B **67**, 195107 (2003).

[28] W. Hanke, Phys. Rev. B **8**, 4585 (1973).

[29] S. Vosko, J. Perdew, and A. MacDonald, Phys. Rev. Lett. **35**, 1725 (1975).

[30] O. Gunnarsson, J. Phys. F: Met. Phys. **6**, 587 (1976).

[31] J. Janak, Phys. Rev. B **16**, 255 (1977).

[32] I. I. Mazin and D. J. Singh, Phys. Rev. B **56**, 2556 (1997).

[33] T. Moriya, *Spin Fluctuations in Itinerant Electron Magnetism*, Springer Ser. Solid-State Science Vol. 56, (Springer, Berlin, 1985).

[34] T. Moriya and K. Ueda, Rep. Prog. Phys. **66**, 1299 (2003).

[35] S. M. Hayden, R. Doubble, G. Aeppli, T. G. Perring, and E. Fawcett, Phys. Rev. Lett. **84**, 999 (2000).

[36] J. M. Bass, J. A. Blackman, and J. F. Cooke, Phys. Rev. B **53**, 2556 (1996).